

LEO Constellations as a Decentralized GNSS Network: Optimizing PNT Corrections in Space

Xing Liu, Xue Xian Zheng, José A. López-Salcedo, *Senior Member, IEEE*, Tareq Y. Al-Naffouri, *Fellow, IEEE*, Gonzalo Seco-Granados, *Fellow, IEEE*

Abstract—With the rapid expansion of low Earth orbit (LEO) constellations, thousands of satellites are now in operation, many equipped with onboard GNSS receivers capable of continuous orbit determination and time synchronization. This development is creating an unprecedented spaceborne GNSS network, offering new opportunities for network-driven precise LEO orbit and clock estimation. Yet, current onboard GNSS processing is largely standalone and often insufficient for high-precision applications, while centralized fusion is challenging due to computational bottlenecks and the lack of in-orbit infrastructure. In this work, we report a decentralized GNSS network over large-scale LEO constellations, where each satellite processes its own measurements while exchanging compact information with neighboring nodes to enable precise orbit and time determination. We model the moving constellation as a dynamic graph and tailor a momentum-accelerated gradient tracking (GT) method to ensure steady convergence despite topology changes. Numerical simulations with constellations containing hundreds of satellites show that the proposed method matches the accuracy of an ideal centralized benchmark, while substantially reducing communication burdens. Ultimately, this framework supports the development of autonomous and self-organizing space systems, enabling high-precision navigation with reduced dependence on continuous ground contact.

Index Terms—LEO constellations, spaceborne GNSS network, decentralized optimization, gradient tracking, orbit determination, time synchronization.

I. INTRODUCTION

LOW Earth orbit (LEO) satellites have become a transformative platform for communications, navigation, remote sensing, Earth observation, and numerous other space applications [1]–[6]. Many of these applications require accurate knowledge of the satellite’s position and clock state, and onboard Global Navigation Satellite System (GNSS) receivers have become a widely used solution for orbit determination and time synchronization [7]–[10]. Currently, most LEO-onboard GNSS processing still relies on standalone positioning using broadcast ephemerides embedded within GNSS signals, which provides only meter-level accuracy due to the limited precision of the broadcast products. Missions requiring higher accuracy instead depend on precise GNSS products generated by International GNSS Service (IGS) analysis centers and

Xing Liu, José A. López-Salcedo, and Gonzalo Seco-Granados are with the Universitat Autònoma de Barcelona (UAB), 08193 Barcelona, Spain. They are also with the Institute for Space Studies of Catalonia (IEEC), Barcelona, Spain.

Xue Xian Zheng and Tareq Y. Al-Naffouri are with the Electrical and Computer Engineering Program, Computer, Electrical and Mathematical Sciences and Engineering Division, King Abdullah University of Science and Technology (KAUST), Thuwal 23955-6900, Saudi Arabia.

Corresponding author: Xue Xian Zheng (xuexian.zheng@kaust.edu.sa).

derived from terrestrial continuously operating reference station (CORS) networks, which provide decimeter to centimeter accuracy [7], [11]. However, such performance is typically achieved only in post-processed orbit determination, since most LEO spacecraft cannot maintain continuous ground connectivity and the latency of precise products limits their usability for real-time operations [7], [8]. Consequently, broadcast ephemerides offer real-time availability but limited positioning accuracy, whereas precise products deliver substantially higher accuracy at the cost of latency and intermittent accessibility. An increasing number of LEO missions, including location-enabled communication systems, formation flying, positioning, navigation, and timing (PNT) services, satellite altimetry, and spaceborne sensing, now require real-time precise orbit and clock determination [7]. Bridging this accuracy-latency gap requires a new architecture capable of delivering both high precision and real-time availability.

Ground-based GNSS networks demonstrate the effectiveness of cooperative processing: observations from global CORS networks are jointly processed at centralized analysis centers to generate precise satellite clocks and orbits, atmospheric corrections, and bias models, which underpin high-precision positioning techniques such as precise point positioning (PPP) [12], [13] and network-assisted PPP real-time kinematic (PPP-RTK) [14]. Modern LEO constellations equipped with onboard GNSS receivers can, in principle, be viewed as a spaceborne analogue of such networks, in which hundreds or thousands of rapidly moving satellites collectively provide a global and geometry-rich set of GNSS observations, as conceptually illustrated in Figure 1. However, existing LEO onboard GNSS receivers typically operate independently: GNSS-derived information is not exchanged among satellites, orbit and clock states are not estimated at the constellation level, and cooperative onboard processing across the constellation remains largely unexplored [7]. Inspired by the success of terrestrial CORS networks, this work examines whether a LEO constellation can operate cooperatively to jointly estimate its orbit and clock states and to generate network-derived GNSS correction information directly onboard. Such a system could extend network-based GNSS processing to the space segment and enable the onboard generation of network-derived GNSS satellite clock corrections, which may serve as a supporting component for high-precision positioning applications, particularly in remote or otherwise challenging environments.

LEO provides a particularly favorable environment for spaceborne GNSS-based inference. Operating above the dense layers of the atmosphere, LEO satellites are effectively free from tropospheric delay, experience substantially reduced



Fig. 1. Conceptual illustration of a LEO constellation viewed as a decentralized spaceborne GNSS network. LEO satellites (bright nodes) form a sparse, time-varying inter-satellite communication graph, while each LEO node receives signals from visible GNSS satellites.

ionospheric effects due to shorter signal propagation paths, and are largely unaffected by multipath [8], [15]. As a result, GNSS measurements collected in LEO are considerably cleaner than those obtained by ground-based receivers. In addition, the high orbital velocity of LEO spacecraft induces strong Doppler signatures and rapidly varying observation geometry, both of which enhance measurement observability and render Doppler a highly informative and complementary observable [16]. The scale of modern LEO constellations further amplifies these advantages, as thousands of rapidly moving satellites naturally provide dense global coverage and rich geometric diversity.

Despite these favorable observation conditions, realizing cooperative orbit and clock estimation at the constellation level is fundamentally challenged by the dynamic nature of LEO networks. Satellite visibility and inter-satellite connectivity vary over time, while scaling to thousands of satellites dramatically increases the density of observations, placing stringent demands on update rates [17], [18]. These characteristics give rise to a large-scale, communication-constrained network with limited bandwidth and time-varying connectivity. Under these constraints, centralized processing is challenging: it incurs excessive communication and computational burdens, introduces significant latency, and ultimately fails to scale with constellation size. Moreover, no such spaceborne fusion center currently exists, and establishing one for constellation-wide processing would require substantial cost and dedicated infrastructure. Together, these challenges motivate a decentralized processing paradigm, in which each LEO satellite performs local estimation based on its own observations and exchanges only compact information with neighboring nodes over a time-varying communication graph.

With sufficient connectivity, decentralized estimation offers a pathway to globally consistent solutions without forward-

ing raw measurements to a centralized analysis center. By shifting computation toward the data sources, such approaches reduce backhaul load, lower latency, and enable inherent parallelism with more efficient resource utilization [19]–[22]. Beyond these benefits, decentralized architectures alleviate communication and computational burdens, improve scalability, enhance resilience to node or link failures, preserve data locality, and support higher update rates as observation density increases [23]. These properties make decentralized processing a promising direction for large, dynamic LEO constellations operating as cooperative GNSS observation networks. Nevertheless, achieving decentralized estimation that ensures system-wide coordination remains challenging in large-scale, communication-constrained LEO networks.

Based on these considerations, this work investigates the idea of treating a LEO constellation as a decentralized spaceborne GNSS network, in which onboard GNSS receivers cooperatively estimate constellation-level states to enable precise LEO orbit and clock determination. In this formulation, each satellite operates as a node in a time-varying communication graph and contributes its locally collected GNSS observations to a constellation-wide estimation process. This perspective naturally leads to a decentralized estimation framework designed to accommodate the large scale and high dynamics of LEO constellations, as well as the intermittent connectivity inherent to onboard operations.

The main contributions of this work are as follows:

- 1) We propose a spaceborne GNSS network architecture for large-scale LEO constellations, in which LEO satellites cooperatively process shared GNSS information to perform precise self-orbit and clock determination in a fully decentralized manner. This architecture allows precise on-orbit estimation of orbit and clock states through cooperative processing.

- 2) We model the inter-satellite communication topology induced by LEO orbital dynamics as a time-varying but predictable graph, and develop a momentum-accelerated gradient tracking (GT) algorithm tailored to this setting. This approach significantly improves convergence rates, thereby drastically reducing the communication overhead required to reach a specific error tolerance.
- 3) We provide a large-scale numerical evaluation with hundreds of LEO satellites, demonstrating that decentralized precise orbit and clock determination can achieve accuracy comparable to centralized processing. These findings suggest a viable path toward large-scale on-orbit computing infrastructures where scalability and varying communication patterns are first-order design constraints.

The remainder of this paper is organized as follows. Section II introduces the spaceborne GNSS observation model. Section III analyzes the estimability of parameters in LEO onboard GNSS networks. Section IV presents the proposed decentralized estimation algorithm for time-varying inter-satellite communication topologies. Section V reports numerical results that demonstrate the feasibility of the proposed approach. Section VI concludes the paper.

II. SPACEBORNE GNSS OBSERVATION EQUATIONS

LEO satellites, whose orbital altitudes typically range from 300 to 1500 km, experience high relative dynamics with GNSS satellites, producing Doppler shifts of up to tens of kilohertz. These strong Doppler dynamics provide rich information content and, when properly modeled, improve the observability of orbit, velocity, and onboard clock states, in contrast to ground receivers, which observe only weak Doppler variations. In addition, LEO satellites operate above the troposphere, so no tropospheric delay is present, and their much shorter ionospheric path greatly reduces ionospheric delay. Together, the high dynamics and simplified propagation conditions create an observation environment that differs from that of ground-based GNSS.

In the proposed spaceborne GNSS networked framework, a large LEO constellation is modeled as a network of spaceborne GNSS receiver nodes. Each LEO satellite is equipped with an onboard GNSS receiver that tracks signals transmitted by GNSS satellites. Consider a system consisting of L LEO satellites and G GNSS satellites. Due to orbital geometry and line-of-sight (LOS) visibility, each receiver has access to only a subset of the GNSS constellation at a given epoch. When receiver l observes transmitter g , the linearized observation equations on frequency f can be written in unified form as:

$$\begin{aligned} \mathbb{E}\left\{\Delta\phi_{l,f}^g\right\} &= (\mathbf{u}_l^g)^T \Delta\mathbf{p}_l + \Delta t_l + \lambda_f \delta_{l,f} - \Delta t_l \\ &\quad - \lambda_f \delta_f^g - \mu_f I_l^g + \lambda_f z_{l,f}^g, \\ \mathbb{E}\left\{\Delta\rho_{l,f}^g\right\} &= (\mathbf{u}_l^g)^T \Delta\mathbf{p}_l + \Delta t_l + b_{l,f} - \Delta t_l \\ &\quad - b_f^g + \mu_f I_l^g, \\ \mathbb{E}\left\{\Delta d_{l,f}^g\right\} &= -\frac{1}{\lambda_f} (\mathbf{u}_l^g)^T \Delta\mathbf{v}_l - \frac{1}{\lambda_f} (\Delta t_l - \Delta t_l^g) \\ &\quad - \frac{\mu_f}{\lambda_f} \dot{I}_l^g, \end{aligned} \quad (1)$$

where $\mathbb{E}\{\cdot\}$ denotes expectation, and

- $\Delta\phi_{l,f}^g$, $\Delta\rho_{l,f}^g$, and $\Delta d_{l,f}^g$ denote the undifferenced observed-minus-computed carrier-phase, pseudorange (code), and Doppler measurements, respectively.
- $l = 1, \dots, L$, $g = 1, \dots, G$, and $f = 1, \dots, F$ index the LEO receivers, GNSS satellites, and frequencies.
- \mathbf{u}_l^g denotes the line-of-sight (LOS) unit vector from GNSS satellite g to receiver l .
- $\Delta\mathbf{p}_l$ and $\Delta\mathbf{v}_l$ represent the incremental position and velocity of receiver l , respectively.
- Δt_l and Δt_l^g denote the receiver and GNSS satellite clock biases, with Δt_l and Δt_l^g representing the corresponding clock drift terms.
- $\delta_{l,f}$ and δ_f^g denote the receiver and GNSS satellite carrier-phase hardware biases at frequency f , while $b_{l,f}$ and b_f^g denote the corresponding pseudorange hardware biases.
- I_l^g represents the ionospheric delay at the first frequency, scaled to frequency f by $\mu_f = \lambda_f^2/\lambda_1^2$. The ionospheric delay rate \dot{I}_l^g is neglected in the subsequent analysis.
- $z_{l,f}^g$ denotes the carrier-phase ambiguity.

To construct the network-wide observation vector, the observables are ordered as follows. For each receiver l , the measurements are grouped by frequency: starting from $f = 1$, all carrier-phase observations are listed first, followed by all pseudorange observations, and then all Doppler observations. Within each observation type, satellites are arranged according to the prescribed satellite ordering. The same structure is repeated for frequencies 2 through F , and then for receivers 1 through L . With this data organization, the network-wide observation vector is defined as

$$\mathbf{y} = [\mathbf{y}_1^T, \dots, \mathbf{y}_L^T]^T, \quad (2)$$

where \mathbf{y}_l collects the measurements associated with receiver l and is structured as

$$\mathbf{y}_l = [\mathbf{y}_{l,1}^T, \dots, \mathbf{y}_{l,F}^T]^T, \quad \mathbf{y}_{l,f} = [\Delta\phi_{l,f}^T, \Delta\rho_{l,f}^T, \Delta d_{l,f}^T]^T.$$

Here, $\Delta\phi_{l,f}$, $\Delta\rho_{l,f}$, $\Delta d_{l,f} \in \mathbb{R}^{G_l}$ contain the frequency- f observations from the G_l GNSS satellites visible to receiver l (with $G_l < G$).

The unknown parameters of the considered spaceborne GNSS system can be grouped into five physically meaningful categories:

- **LEO orbit-related states:** incremental position and velocity corrections of the LEO satellites.

$$\mathbf{x}_{\text{leo-orb}} = \text{col}\{\Delta\mathbf{p}_1, \Delta\mathbf{v}_1, \dots, \Delta\mathbf{p}_L, \Delta\mathbf{v}_L\} \in \mathbb{R}^{6L},$$

where $\text{col}\{\cdot\}$ denotes the column-wise concatenation.

- **LEO clock and hardware-related states:** onboard receiver clock offsets and drifts, and carrier-phase and pseudorange hardware biases for each frequency.

$$\mathbf{x}_{\text{leo-clk}} = \text{col}\{\mathbf{x}_{\text{leo-clk}}^{(1)}, \dots, \mathbf{x}_{\text{leo-clk}}^{(L)}\} \in \mathbb{R}^{L(2+2F)},$$

with

$$\mathbf{x}_{\text{leo-clk}}^{(l)} = [\Delta t_l, \Delta \dot{t}_l, \delta_{l,1}, \dots, \delta_{l,F}, b_{l,1}, \dots, b_{l,F}]^T.$$

- **GNSS clock and hardware-related states:** GNSS satellite clock offsets and drifts, together with transmitter carrier-phase and pseudorange hardware biases.

$$\mathbf{x}_{\text{gnss-clk}} = \text{col} \{ \mathbf{x}_{\text{gnss-clk}}^{(1)}, \dots, \mathbf{x}_{\text{gnss-clk}}^{(g)} \} \in \mathbb{R}^{G(2+2F)},$$

with

$$\mathbf{x}_{\text{gnss-clk}}^{(g)} = [\Delta t^g, \Delta \dot{t}^g, \delta_1^g, \dots, \delta_F^g, b_1^g, \dots, b_F^g]^T.$$

- **Ionosphere-related states:** ionospheric delays associated with each observable LEO–GNSS link.

$$\mathbf{x}_{\text{ion}} = \text{col} \{ \mathbf{x}_{\text{ion}}^{(1)}, \dots, \mathbf{x}_{\text{ion}}^{(L)} \} \in \mathbb{R}^{\sum_l G_l},$$

where

$$\mathbf{x}_{\text{ion}}^{(l)} = [I_l^{g_1}, \dots, I_l^{g_{G_l}}]^T \in \mathbb{R}^{G_l}.$$

- **Integer ambiguities:** carrier-phase ambiguities for all LEO–GNSS links and frequencies.

$$\mathbf{x}_{\text{amb}} = \text{col} \{ \mathbf{x}_{\text{amb}}^{(1)}, \dots, \mathbf{x}_{\text{amb}}^{(L)} \} \in \mathbb{R}^{\sum_l FG_l},$$

with

$$\mathbf{x}_{\text{amb}}^{(l)} = \{ \mathbf{x}_{\text{amb}}^{(l,1)}, \dots, \mathbf{x}_{\text{amb}}^{(l,F)} \} \in \mathbb{R}^{FG_l},$$

$$\mathbf{x}_{\text{amb}}^{(l,f)} = [z_{l,f}^{g_1}, \dots, z_{l,f}^{g_{G_l}}]^T \in \mathbb{R}^{G_l}.$$

The vector of unknown parameters is then represented as

$$\mathbf{x} = [\mathbf{x}_{\text{leo-orb}}^T, \mathbf{x}_{\text{leo-clk}}^T, \mathbf{x}_{\text{gnss-clk}}^T, \mathbf{x}_{\text{ion}}^T, \mathbf{x}_{\text{amb}}^T]^T. \quad (3)$$

Given the definitions of \mathbf{y} and \mathbf{x} , the linearized network-wide observation model can be written as

$$\mathbf{y} = \mathbf{Ax}. \quad (4)$$

Following the same five-state grouping introduced for \mathbf{x} , the corresponding design matrix is structured as

$$\mathbf{A} = [\mathbf{A}_{\text{leo-orb}} \mid \mathbf{A}_{\text{leo-clk}} \mid \mathbf{A}_{\text{gnss-clk}} \mid \mathbf{A}_{\text{ion}} \mid \mathbf{A}_{\text{amb}}]. \quad (5)$$

The submatrices appearing in (5) are defined in Appendix A.

The GNSS satellite-specific parameters $\mathbf{x}_{\text{gnss-clk}}$ constitute shared global states, while all remaining parameters are receiver-related and treated as local states. This local–global parameter structure naturally leads to a network-driven precise estimation formulation, in which the global states are inferred cooperatively across the LEO constellation. The resulting global states provide a consistent reference that supports precise determination of the local LEO orbit and clock states, namely $\mathbf{x}_{\text{leo-orb}}$ for LEO orbit determination and $\mathbf{x}_{\text{leo-clk}}$ for constellation-wide time synchronization. In this sense, the derived GNSS satellite clock states $\mathbf{x}_{\text{gnss-clk}}$ can be interpreted as GNSS satellite clock correction information generated by the LEO network, which may serve as a potential correction source for downstream GNSS positioning applications. The estimability of the individual parameter components, and the conditions under which they can be uniquely identified, are discussed in the next section.

III. ESTIMABILITY AND IDENTIFIABILITY ANALYSIS OF MODEL PARAMETERS

The observation equations introduced in Section II inherently lead to a rank-deficient estimation problem: the design matrix \mathbf{A} is not full rank, meaning that only certain linear combinations of the parameters are identifiable, while their absolute values are not. For a networked architecture, this issue is particularly critical, as all nodes must adopt a common set of physically meaningful estimable parameters; otherwise, different nodes would converge to mutually inconsistent solutions. To address this challenge, we adopt the \mathcal{S} -system theory to rigorously characterize the identifiable parameter combinations of the proposed spaceborne GNSS network [24]–[26].

To identify the rank deficiencies of the design matrix in (4), we examine which changes in the unknown parameters leave all measurements unchanged. A straightforward example is a common shift applied simultaneously to all receiver clocks and all GNSS satellite clocks, which does not affect either the carrier-phase or pseudorange observations. It indicates that the corresponding clock parameters are not independently observable. Such a dependency introduces a rank deficiency, which can be resolved by designating one receiver clock as the temporal reference, thereby removing it from the set of unknowns. This constraint forms part of the adopted \mathbf{S} -basis.

Applying the same reasoning to the full model reveals additional parameter dependencies. These dependency categories, together with the specific constraints used to eliminate them, are summarized in TABLE I. For clarity, let n and m denote the dimensions of the unknown parameter vector \mathbf{x} and the observation vector \mathbf{y} , respectively. Thus, $\mathbf{y} \in \mathbb{R}^m$, $\mathbf{x} \in \mathbb{R}^n$, and the corresponding design matrix satisfies $\mathbf{A} \in \mathbb{R}^{m \times n}$ with $\text{rank}(\mathbf{A}) = r \leq n$. The total dimension of the associated null space, i.e., the cumulative size of all rank deficiencies, is

$$n - r = 2 + 2F + (L - 1 + G). \quad (6)$$

The range and null spaces of the matrix \mathbf{A} are denoted by $\mathcal{R}(\mathbf{A})$ and $\mathcal{N}(\mathbf{A})$, with dimensions $\dim \mathcal{R}(\mathbf{A}) = r$ and $\dim \mathcal{N}(\mathbf{A}) = n - r$, respectively. Let $\mathbf{V} \in \mathbb{R}^{n \times (n-r)}$ be a matrix whose columns form a basis of the null space $\mathcal{N}(\mathbf{A})$, so that $\mathbf{AV} = \mathbf{0}$. Although the null space $\mathcal{N}(\mathbf{A})$ is unique, the particular choice of its basis matrix \mathbf{V} is not. Let $\mathbf{S} \in \mathbb{R}^{n \times r}$ denote a basis matrix spanning a subspace complementary to $\mathcal{R}(\mathbf{V})$, such that

$$\mathbb{R}^n = \mathcal{R}(\mathbf{S}) \oplus \mathcal{R}(\mathbf{V}).$$

Because the matrix \mathbf{A} is rank-deficient, i.e., $r < n$, the observations do not contain sufficient information to determine all components of the parameter vector. In this case, \mathbf{x} can be decomposed into two parts: an estimable component $\mathbf{x}_s \in \mathcal{R}(\mathbf{S})$ and a non-estimable component $\mathbf{x}_v \in \mathcal{R}(\mathbf{V})$. This decomposition can be written as

$$\mathbf{x} = \underbrace{\mathbf{S}\alpha}_{\mathbf{x}_s} + \underbrace{\mathbf{V}\beta}_{\mathbf{x}_v} = [\mathbf{S} \quad \mathbf{V}] \begin{bmatrix} \alpha \\ \beta \end{bmatrix}, \quad (7)$$

where $\alpha \in \mathbb{R}^r$ contains the estimable parameter functions associated with \mathbf{S} , and $\beta \in \mathbb{R}^{n-r}$ contains the inestimable parameter functions associated with \mathbf{V} .

Since the square matrix $[\mathbf{S} \quad \mathbf{V}] \in \mathbb{R}^{n \times n}$ is invertible, the coefficients α and β can be obtained from

$$\begin{bmatrix} \alpha \\ \beta \end{bmatrix} = [\mathbf{S} \quad \mathbf{V}]^{-1} \mathbf{x} = \begin{bmatrix} [(\mathbf{V}^\perp)^T \mathbf{S}]^{-1} (\mathbf{V}^\perp)^T \\ [(\mathbf{S}^\perp)^T \mathbf{V}]^{-1} (\mathbf{S}^\perp)^T \end{bmatrix} \mathbf{x}. \quad (8)$$

Here, $\mathbf{V}^\perp \in \mathbb{R}^{n \times r}$ is a basis matrix whose columns span a subspace orthogonal to $\mathcal{R}(\mathbf{V})$, satisfying $(\mathbf{V}^\perp)^T \mathbf{V} = \mathbf{0}$. Similarly, $\mathbf{S}^\perp \in \mathbb{R}^{n \times (n-r)}$ is defined such that $(\mathbf{S}^\perp)^T \mathbf{S} = \mathbf{0}$.

Based on the chosen basis matrices \mathbf{S} and \mathbf{V} , the observation model becomes a full-rank system in the estimable parameters α :

$$E\{\mathbf{y}\} = \mathbf{A}(\mathbf{S}\alpha + \mathbf{V}\beta) = \underbrace{(\mathbf{A}\mathbf{S})}_{\mathbf{A}} \alpha. \quad (9)$$

This identifies the estimable component of \mathbf{x} as

$$\mathbf{x}_S = \mathbf{S}\alpha = \mathbf{x} - \mathbf{V}\beta = \mathcal{S}\mathbf{x}, \quad (10)$$

where $\mathcal{S} \in \mathbb{R}^{n \times n}$ denotes the \mathcal{S} -transformation matrix. It admits the equivalent representations

$$\begin{aligned} \mathcal{S} &= \mathbf{S} [(\mathbf{V}^\perp)^T \mathbf{S}]^{-1} (\mathbf{V}^\perp)^T \\ &= \mathbf{I}_n - \mathbf{V} [(\mathbf{S}^\perp)^T \mathbf{V}]^{-1} (\mathbf{S}^\perp)^T. \end{aligned} \quad (11)$$

The matrix \mathcal{S} therefore defines the linear combinations of the initial parameters that can be estimated based on the chosen \mathbf{S} -basis.

Different choices of the \mathbf{S} -basis may be adopted, with each choice defining a particular set of estimable global products and LEO-specific states. TABLE I presents the selection of \mathbf{S} -basis constraints used in this work to eliminate the rank deficiencies. The corresponding matrices \mathbf{S} , \mathbf{V} , $(\mathbf{S}^\perp)^T$, and \mathcal{S} are provided in Appendix B, where they are organized into five column blocks consistent with the five parameter groups in the network model. Then, we can obtain a full-rank, undifferenced spaceborn GNSS network model. The resulting parameters are no longer the original absolute states

but their estimable linear combinations, denoted by the symbol $(\tilde{\cdot})$. Table II summarizes these estimable network parameters and clarifies their interpretation under the adopted \mathbf{S} -basis following the corresponding \mathcal{S} -transformation. The carrier-phase ambiguities are transformed into a double-differenced form, in which the initial phase terms are eliminated and the resulting ambiguities are integer-valued, thereby enabling integer-constrained high-precision positioning.

Please note that, for simplicity, the epoch index has been omitted in the above formulations. Following standard multi-epoch undifferenced GNSS modeling, the observation equations can be stacked over multiple epochs, where time variation enters through changing geometry and satellite visibility. Importantly, the \mathbf{S} -basis identified from a single-epoch formulation applies equally to the stacked multi-epoch model and fully characterizes the set of estimable parameter combinations. To avoid unnecessary complexity, an explicit multi-epoch formulation is not provided here. The objective of this section is to present the fundamental methodology for establishing a well-defined estimation problem under the proposed spaceborne GNSS network model, which underpins the decentralized estimation framework developed later.

IV. NETWORK MODEL FOR LEO ONBOARD GNSS PROCESSING

In this section, we introduce a networked onboard processing framework for LEO constellations. Building on the analysis in the previous sections, we derive a well-defined decentralized problem formulation in which all nodes estimate a common set of identifiable parameters, enabling consistent network-wide estimation for onboard processing. We then develop a momentum-accelerated gradient tracking (GT) algorithm to solve the resulting problem. The proposed approach is explicitly tailored to the orbital dynamics and inter-satellite communication constraints of LEO constellations.

TABLE I
RANK DEFICIENCIES IN SPACEBORNE GNSS NETWORK: TYPES, SIZES, AND THE \mathbf{S} -BASIS CONSTRAINTS CHOSEN FOR THEIR ELIMINATION

Rank-deficiency Type	Size	Chosen \mathbf{S} -basis Constraint	Notation
Between LEO receiver and GNSS satellite clocks	1	Pivot receiver clock	Δt_1
Between LEO receiver and GNSS satellite clock drift	1	Pivot receiver clock drift	$\Delta \dot{t}_1$
Between LEO receiver and GNSS satellite hardware biases	$2F$	Pivot receiver hardware biases	$\begin{cases} \delta_{1,f} & f \geq 1 \\ b_{1,f} & \end{cases}$
Between LEO receiver clocks and receiver hardware biases	$L - 1$	Ionosphere-free receiver code biases	$b_{l,\text{IF}}, l \geq 2$
Between GNSS satellite clocks and hardware biases	G	Ionosphere-free satellite code biases	$b_{\text{IF}}^g, g \geq 1$
Between LEO receiver hardware biases and ionospheric delays	$L - 1$	Geometry-free receiver code biases	$b_{l,\text{GF}}, l \geq 2$
Between GNSS satellite hardware biases and ionospheric delays	G	Geometry-free satellite code biases	$b_{\text{GF}}^g, g \geq 1$
Between LEO receiver hardware biases and ambiguities	$F(L - 1)$	Carrier-phase ambiguities for pivot satellites	$z_{l,f}^{p(l)}, l \geq 2, f \geq 1$
Between GNSS satellite hardware biases and ambiguities	FG	Carrier-phase ambiguities for pivot receivers	$z_{l_p(g),f}^g, g \geq 1, f \geq 1$

* $b_{l,\text{IF}} = \frac{\mu_2}{\mu_2 - \mu_1} b_{l,1} - \frac{\mu_1}{\mu_2 - \mu_1} b_{l,2}$, $b_{\text{IF}}^g = \frac{\mu_2}{\mu_2 - \mu_1} b_1^g - \frac{\mu_1}{\mu_2 - \mu_1} b_2^g$, $b_{l,\text{GF}} = \frac{1}{\mu_2 - \mu_1} [b_{l,2} - b_{l,1}]$, $b_{\text{GF}}^g = \frac{1}{\mu_2 - \mu_1} [b_2^g - b_1^g]$

TABLE II
ESTIMABLE NETWORK PARAMETERS AND THEIR INTERPRETATION USING THE CHOSEN **S**-BASIS

Estimable parameter	Notation and interpretation	Condition
LEO receiver position	$\Delta\tilde{\mathbf{p}}_l = \Delta\mathbf{p}_l$	$l \geq 1$
LEO receiver velocity	$\Delta\tilde{\mathbf{v}}_l = \Delta\mathbf{v}_l$	$l \geq 1$
LEO receiver clock	$\Delta\tilde{t}_l = [\Delta t_l + b_{l,\text{IF}}] - [\Delta t_1 + b_{1,\text{IF}}]$	$l \geq 2$
LEO receiver clock drift	$\Delta\tilde{t}_l = \Delta t_l - \Delta t_1$	$l \geq 2$
LEO receiver phase bias	$\tilde{\delta}_{l,f} = \left[\delta_{l,f} - \frac{1}{\lambda_f} b_{l,\text{IF}} \right] - \left[\delta_{1,f} - \frac{1}{\lambda_f} b_{1,\text{IF}} \right] + \frac{1}{\lambda_f} \mu_f [b_{l,\text{GF}} - b_{1,\text{GF}}] + [z_{l,f}^{g_p(l)} - z_{l_p(g),f}^{g_p(l)}]$	$l \geq 2, f \geq 1$
LEO receiver code bias	$\tilde{b}_{l,f} = [b_{l,f} - b_{l,\text{IF}}] - [b_{1,f} - b_{1,\text{IF}}] - \mu_f [b_{l,\text{GF}} - b_{1,\text{GF}}]$	$l \geq 2, f \geq 3$
GNSS satellite clock	$\Delta\tilde{t}^g = [\Delta t^g + b_{\text{IF}}^g] - [\Delta t_1 + b_{1,\text{IF}}]$	$g \geq 1$
GNSS satellite clock drift	$\Delta\tilde{t}^g = \Delta t^g - \Delta t_1$	$g \geq 1$
GNSS satellite phase bias	$\tilde{\delta}_j^g = \left[\delta_j^g - \frac{1}{\lambda_f} b_{\text{IF}}^g \right] - \left[\delta_{1,f} - \frac{1}{\lambda_f} b_{1,\text{IF}} \right] + \frac{1}{\lambda_f} \mu_f [b_{\text{GF}}^g - b_{1,\text{GF}}] - z_{l_p(g),f}^g$	$g \geq 1, f \geq 1$
GNSS satellite code bias	$\tilde{b}_f^g = [b_f^g - b_{\text{IF}}^g] - [b_{1,f} - b_{1,\text{IF}}] - \mu_f [b_{\text{GF}}^g - b_{1,\text{GF}}]$	$g \geq 1, f \geq 3$
Ionospheric delay	$\tilde{l}_l^g = l_l^g + b_{l,\text{GF}} - b_{\text{GF}}^g$	$l \geq 1, g \geq 1$
Carrier-phase ambiguity	$\tilde{z}_{l,f}^g = [z_{l,f}^g - z_{l,f}^{g_p(l)}] - [z_{l_p(g),f}^g - z_{l_p(g),f}^{g_p(l)}]$	$l \neq l_p(g), g \neq g_p(l), f \geq 1$

A. Well-defined Decentralized Formulation

Upon the full-rank design matrix from Section III, the identifiable parameter vector admits a centralized weighted least-squares formulation, which serves as a natural reference solution:

$$\min_{\tilde{\mathbf{x}}} \|\mathbf{y} - \tilde{\mathbf{A}}\tilde{\mathbf{x}}\|_{\mathbf{Q}^{-1}}^2, \quad (12)$$

where \mathbf{Q} denotes the observation-noise covariance matrix.

However, such a centralized architecture is challenging for large LEO constellations. Transmitting full datasets to a fusion center and forming global normal equations does not scale with constellation size or observation duration, and introduces prohibitive communication, latency, and robustness challenges. These limitations motivate a decentralized formulation in which each LEO node performs local computation while exchanging only compact information with its neighbors.

Guided by the estimability analysis, which specifies the structure of the local variables \mathbf{x}_l and the shared global variable \mathbf{z} , as well as their corresponding local design matrices \mathbf{A}_l and \mathbf{B}_l , each node can locally construct its estimation model based on the common **S**-basis, without ever forming the full network design matrix. Under the decentralized setting, each node requires only its local observations \mathbf{y}_l together with its own local design matrices \mathbf{A}_l and \mathbf{B}_l , without access to other nodes' measurements or the global design matrix. The only information shared across nodes is the selected **S**-basis, which ensures a common estimable parameter space and enables each node to locally construct its corresponding design matrices.

Accordingly, an equivalent yet scalable decentralized formulation can be given by

$$\underset{\{\mathbf{x}_l\}_{l=1}^L, \mathbf{z}}{\text{minimize}} \quad f(\{\mathbf{x}_l\}_{l=1}^L, \mathbf{z}) = \sum_{l=1}^L f_l(\mathbf{x}_l, \mathbf{z}), \quad (13)$$

$$\text{where } f_l(\mathbf{x}_l, \mathbf{z}) = \frac{1}{2} \|\mathbf{A}_l \mathbf{x}_l + \mathbf{B}_l \mathbf{z} - \mathbf{y}_l\|_{\mathbf{Q}^{-1}}^2,$$

where \mathbf{Q}_l is the local measurement noise covariance matrix.

With the above construction, a well-defined decentralized estimation formulation is established. The fundamental challenge is then to ensure that the decentralized optimization remains equivalent to the centralized estimator, such that all nodes reach agreement on the shared global state and converge to the centralized solution through compact neighbor-to-neighbor information exchange. The subsequent subsection describes the mechanisms by which this agreement is achieved.

B. Momentum-Accelerated Gradient Tracking with Orbit Dynamics

We introduce a communication-efficient method to solve (13). Building upon the GT framework [27], which enables decentralized optimization of coupled local objectives by tracking the network-wide gradient using only local information exchange, we incorporate Heavy-ball momentum to accelerate convergence. This acceleration reduces the communication overhead required to reach a target accuracy. As illustrated in Figure 2, we characterize the inter-satellite communication topology of LEO constellations as exhibiting distinct behaviors across two time scales: on a small time scale, the network topology remains effectively invariant, as communication links persist despite the continuous motion of the satellites; on a large time scale, the topology evolves as satellites gradually drift out of range of previous neighbors and establish new connections. Consequently, since the constellation operates iteratively through these regimes, we model the optimization scheme over a piecewise-invariant graph.

Let us assume the optimization of (13) spans a sequence of graphs $\{\mathcal{G}^{(t)} = (\mathcal{V}, \mathcal{E}^{(t)}, \mathbf{W}^{(t)})\}_{t=1}^T$, where each $\mathcal{G}^{(t)}$ dominates a specific time period. Here L LEO satellites form the node set $\mathcal{V} = \{1, \dots, L\}$, while the edge set $\mathcal{E}^{(t)} \subseteq \mathcal{V} \times \mathcal{V}$ represents time-varying inter-satellite communication links.

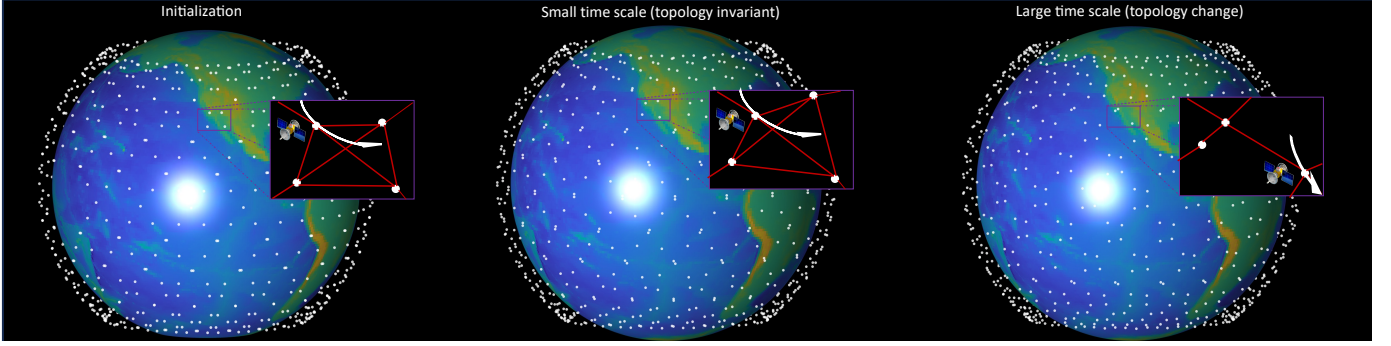


Fig. 2. LEO constellation communication topology across two time scales. Over short horizons, the topology is effectively invariant as links persist despite satellite motion; over longer horizons, the topology changes as satellites move out of range of previous neighbors and establish new links. This motivates modeling the optimization over a periodically invariant (piecewise static) graph sequence $\{\mathcal{G}^{(t)}\}_{t=1}^T$.

The mixing matrix $\mathbf{W}^{(t)} = [w_{lq}^{(t)}] \in \mathbb{R}^{L \times L}$ is compatible with the topology, i.e., $w_{lq}^{(t)} > 0$ only if $(l, q) \in \mathcal{E}^{(t)}$ (or $l = q$), and we assume $\mathbf{W}^{(t)}$ is doubly stochastic: $\mathbf{W}^{(t)}\mathbf{1} = \mathbf{1}$ and $\mathbf{1}^\top \mathbf{W}^{(t)} = \mathbf{1}^\top$. We adopt Metropolis weights for $\mathbf{W}^{(t)}$, which can be computed in a decentralized manner by exchanging node-degree information. Specifically, letting $\mathcal{N}_l^{(t)} = \{q \in \mathcal{V} : (l, q) \in \mathcal{E}^{(t)}\}$ denote the neighbor set of node l and $d_l^{(t)} = |\mathcal{N}_l^{(t)}|$ its degree, the weights are

$$w_{lq}^{(t)} = \begin{cases} \frac{1}{\max(d_l^{(t)}, d_q^{(t)}) + 1} & \text{if } q \in \mathcal{N}_l^{(t)}, \\ 1 - \sum_{p \in \mathcal{N}_l^{(t)}} w_{lp}^{(t)} & \text{if } l = q, \\ 0 & \text{otherwise.} \end{cases} \quad (14)$$

Then, for iteration k within the time period dominated by $\mathcal{G}^{(t)}$, the algorithm at node l proceeds as follows

$$\mathbf{v}_l^k = \mathbf{z}_l^k + \theta (\mathbf{z}_l^k - \mathbf{z}_l^{k-1}), \quad (15a)$$

$$\mathbf{z}_l^{k+1} = \mathcal{C}(\mathbf{v}_l^k - \gamma \mathbf{g}_l^k, \mathcal{K}), \quad (15b)$$

$$\mathbf{x}_l^{k+1} = (\mathbf{A}_l^\top \mathbf{Q}_l^{-1} \mathbf{A}_l)^{-1} \mathbf{A}_l^\top \mathbf{Q}_l^{-1} (\mathbf{y}_l - \mathbf{B}_l \mathbf{z}_l^{k+1}), \quad (15c)$$

$$\mathbf{g}_l^{k+1} = \sum_{q \in \mathcal{N}_l^{(t)}} w_{ql}^{(t)} \mathbf{g}_q^k + \nabla_{\mathbf{z}} f_l(\mathbf{x}_l^{k+1}, \mathbf{z}_l^{k+1}) - \nabla_{\mathbf{z}} f_l(\mathbf{x}_l^k, \mathbf{z}_l^k), \quad (15d)$$

where $\nabla_{\mathbf{z}} f_l(\mathbf{x}_l, \mathbf{z}_l)$ denotes the gradient of $f_l(\mathbf{x}_l, \mathbf{z}_l)$ with respect to \mathbf{z} .

Under this formulation, (15a) implements the Heavy-ball momentum update \mathbf{v}_l^k with coefficient $\theta \in [0, 1]$; (15b) performs a γ descent step combined with a \mathcal{K} -round consensus operator $\mathcal{C}(\cdot)$ to obtain \mathbf{z}_l^{k+1} ; (15c) computes the closed-form update of the local auxiliary variable \mathbf{x}_l given \mathbf{z}_l^{k+1} (as derived in [28]); and (15d) updates the gradient tracker \mathbf{g}_l^{k+1} . The complete iterative procedure is summarized in Algorithm 1. For simplicity, we assume that each snapshot $\mathcal{G}^{(t)}$ remains dominant for the same period length.

The consensus operator $\mathcal{C}(\cdot)$ performs \mathcal{K} rounds of neighborhood mixing using the mixing matrix $\mathbf{W}^{(t)}$. This design is motivated by LEO constellations, where the inter-satellite communication graph is typically sparse (e.g., each satellite may communicate with only a few neighbors), which leads to poor mixing in a single round. By incorporating multi-round mixing, $\mathcal{C}(\cdot)$ strengthens information diffusion across

Algorithm 1 Momentum-Accelerated GT for LEO GNSS

Require: Graph patterns $\{\mathcal{G}^{(t)}\}_{t=1}^T$; stepsize $\gamma > 0$; momentum θ ; maximum iterations K , consensus rounds \mathcal{K}
Require: Local data $\{\mathbf{A}_l, \mathbf{B}_l, \mathbf{Q}_l, \mathbf{y}_l\}_{l=1}^L$ and f_l as in (13)
Ensure: Estimates $\{\mathbf{x}_l^K, \mathbf{z}_l^K\}_{l=1}^L$

- 1: **Initialization:** For each node l , initialize $\mathbf{z}_l^0 = \mathbf{z}_l^{-1}$, calculate $\mathbf{x}_l^0 \leftarrow (\mathbf{A}_l^\top \mathbf{Q}_l^{-1} \mathbf{A}_l)^{-1} \mathbf{A}_l^\top \mathbf{Q}_l^{-1} (\mathbf{y}_l - \mathbf{B}_l \mathbf{z}_l^0)$, and set $\mathbf{g}_l^0 \leftarrow \nabla_{\mathbf{z}} f_l(\mathbf{x}_l^0, \mathbf{z}_l^0)$
- 2: **for** $k = 0$ **to** $K - 1$ **do**
- 3: $t \leftarrow \lfloor k/T \rfloor + 1$;
- 4: $\mathbf{W}^{(t)} \leftarrow \mathcal{G}^{(t)}$;
- 5: **for all** $l \in \{1, \dots, L\}$ **do**
- 6: $\mathbf{v}_l^k \leftarrow \mathbf{z}_l^k + \theta (\mathbf{z}_l^k - \mathbf{z}_l^{k-1})$;
- 7: $\mathbf{g}_l^k \leftarrow \mathbf{v}_l^k - \gamma \mathbf{g}_l^k$;
- 8: $\varphi_l \leftarrow \mathbf{g}_l^k$;
- 9: **for** $\kappa = 0$ **to** $\mathcal{K} - 1$ **do**
- 10: $\varphi_l \leftarrow \sum_{q \in \mathcal{N}_l^{(t)}} w_{ql}^{(t)} \varphi_q$;
- 11: **end for**
- 12: $\mathbf{z}_l^{k+1} \leftarrow \varphi_l$;
- 13: $\mathbf{x}_l^{k+1} \leftarrow (\mathbf{A}_l^\top \mathbf{Q}_l^{-1} \mathbf{A}_l)^{-1} \mathbf{A}_l^\top \mathbf{Q}_l^{-1} (\mathbf{y}_l - \mathbf{B}_l \mathbf{z}_l^{k+1})$;
- 14: $\mathbf{g}_l^{k+1} \leftarrow \sum_{q \in \mathcal{N}_l^{(t)}} w_{ql}^{(t)} \mathbf{g}_q^k + \nabla_{\mathbf{z}} f_l(\mathbf{x}_l^{k+1}, \mathbf{z}_l^{k+1}) - \nabla_{\mathbf{z}} f_l(\mathbf{x}_l^k, \mathbf{z}_l^k)$;
- 15: **end for**
- 16: **end for**

the network and can stabilize the updates, allowing a larger momentum parameter θ and stepsize γ and thereby improving convergence in practice.

Although multi-round consensus increases the communication cost per iteration, prior works have significantly reduced this overhead via low-bit quantization and error-feedback mechanisms [29], [30]. In such approaches, the multi-round consensus can be interpreted as applying a finite-impulse-response (FIR) graph filter implemented through repeated local exchanges [31], [32]. Moreover, performing consensus-only steps (i.e., mixing without additional gradient evaluations) can reduce the wall-clock time by mitigating straggler effects, which is particularly beneficial when the communication window is short.

V. NUMERICAL RESULTS

Numerical simulations are conducted to evaluate the proposed network-based LEO onboard GNSS processing framework. A Walker-Delta LEO constellation consisting of 500 satellites is considered, where each satellite is equipped with a dual-frequency GNSS receiver. The satellites are deployed in 20 orbital planes with 25 satellites per plane, at an altitude of 550 km and an inclination of 53°, and their trajectories are propagated accordingly. Each LEO satellite is assumed to communicate with its 4 nearest neighbors, thereby forming a sparse, time-varying communication graph for information exchange. GNSS satellite positions are generated by propagating the corresponding orbital parameters. In the simulations, only GPS satellites are considered, with a total of 30 satellites. Dual-frequency observations at the GPS L1/L2 frequencies are simulated, including undifferenced carrier-phase, code pseudorange, and Doppler measurements. An elevation mask of 0° is applied, and only LOS visible GNSS satellites are used at each epoch. Measurement noise is modeled as zero-mean Gaussian, with standard deviations of 1 mm for carrier phase, 10 cm for code, and 0.5 Hz for Doppler. Receiver clock offsets are initialized with a standard deviation of 100 ns, while the GNSS satellite clock offsets are assigned an initial uncertainty of 10 ns. The resulting simulated observation set is used for the subsequent estimation analysis.

For the algorithm settings, the per-epoch processing is assumed to evolve over a graph sequence $\{\mathcal{G}^{(t)}\}_{t=1}^3$ and runs for at most $K_{\max} = 1.2 \times 10^4$ iterations. Unless otherwise specified, we set the stepsize $\gamma = 0.01$, the momentum parameter $\theta = 0.7$, and the number of consensus rounds $\mathcal{K} = 20$, and initialize GNSS satellite parameters as zeros for Algorithm 1. We report the resulting network-based cooperative solution and compare it against a non-cooperative standalone solution in which each satellite processes its own measurements independently.

Figure 3 and Figure 4 compare the orbit determination and time synchronization performance under three processing strategies: standalone per-receiver processing, network-based processing with float ambiguities, and network-based processing with integer-fixed ambiguities. As shown in Figure 3, standalone processing yields a LEO orbit determination error of 2.95 m, reflecting the limited accuracy of individual receivers. By jointly estimating shared GNSS satellite clock states across the constellation, the network-based float solution significantly improves the orbit accuracy to 0.12 m. When integer ambiguity resolution is enabled using the LAMBDA method [33], the network-fixed solution further reduces the orbit error to 0.06 m, achieving centimeter-level accuracy. Figure 4 shows the corresponding time synchronization performance. The standalone solution exhibits a timing error of 7.95 ns. For the network-based solutions, the reported timing errors correspond to the network-consistent clock states. Network-based float processing achieves a timing accuracy of approximately 0.21 ns, which is further improved to 0.11 ns after integer ambiguity fixing. Overall, the results demonstrate that network-based onboard GNSS processing enables substantial gains in both orbit determination and time synchronization,

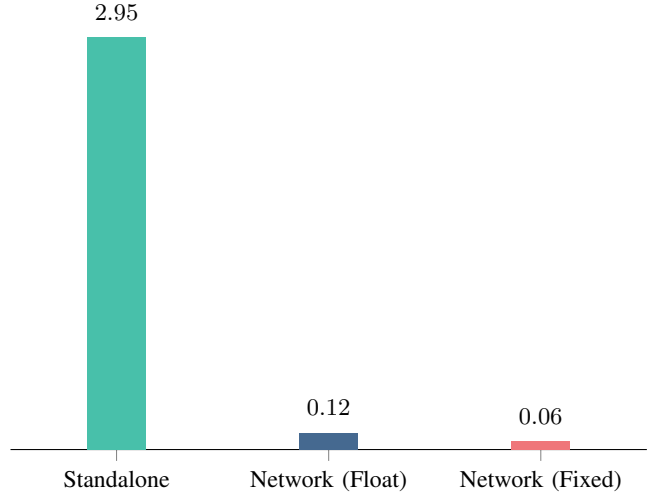


Fig. 3. LEO orbit determination error under different processing strategies (meter).

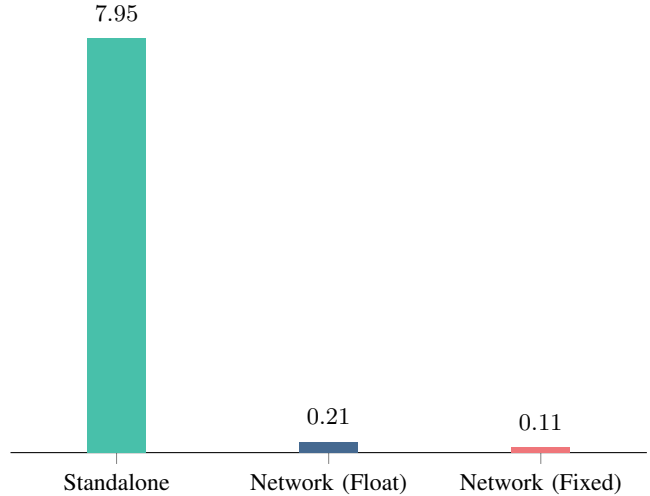


Fig. 4. LEO time synchronization error under different processing strategies (nanosecond).

with integer ambiguity resolution provides further performance improvements.

We characterize the convergence behavior of our algorithm in Figure 5 and Figure 6. The former illustrates the mean-square deviation (MSD) with respect to the centralized solution, while the latter depicts the proximity to first-order optimality (gradient norm). Through an ablation study, we demonstrate that our method converges linearly to the centralized solution with significant acceleration. Crucially, this acceleration stems from the synergy between momentum and multi-round consensus; neither component is sufficient on its own. Specifically, the vanilla GT algorithm is restricted to a quarter of the stepsize due to the sparsely connected underlying graph of the LEO constellations. In this regime, incorporating momentum yields only marginal improvements, as stability constraints force the momentum parameter θ to remain small. However, employing \mathcal{K} consensus rounds reduces the disagreement error between states, enabling the use

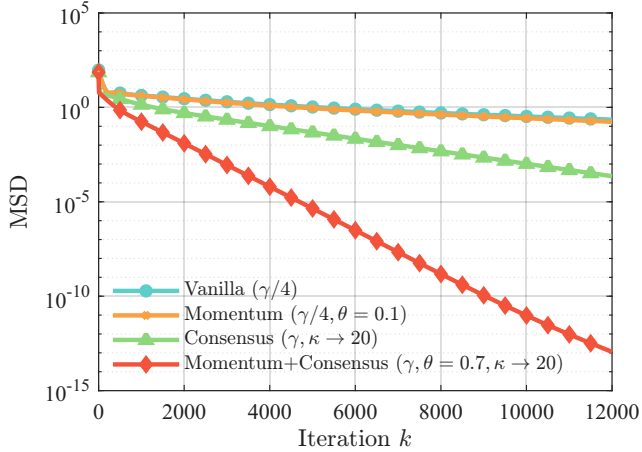


Fig. 5. Convergence behavior measured by MSD. We compare the vanilla GT method with its momentum-accelerated variant, a consensus-only variant, and the combined momentum+consensus scheme. The latter corresponds to our proposed method, while the others serve as ablations.

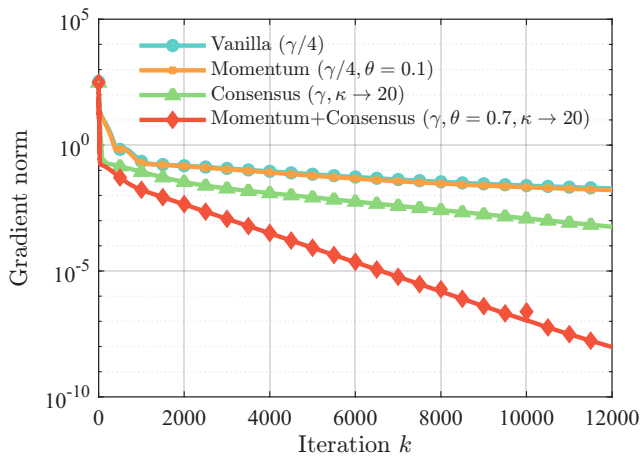


Fig. 6. Evolution of the norm of the network-averaged gradient corresponding to the results in Figure 5. We utilize this metric to evaluate the proximity of the solution to first-order optimality.

of a full stepsize γ . This improved stability accommodates a larger momentum parameter, which significantly accelerates convergence. These results confirm that our algorithm achieves the desired estimation accuracy with reduced overhead for a given tolerance. Ultimately, we show that the proposed method provides a viable and scalable algorithmic framework for GNSS network processing onboard LEO satellites, where centralized processing and communication resources are limited.

VI. CONCLUSION

This paper studied decentralized GNSS network processing for large-scale LEO constellations by modeling the constellation as a cooperative spaceborne network interconnected through inter-satellite links. By exploiting the network structure and the redundancy of GNSS observations across satellites, a network-driven estimation framework was established for joint orbit determination and clock synchronization without centralized data fusion while preserving global consistency.

Numerical results demonstrated that cooperative network processing substantially improves both orbit and clock estimation accuracy compared to standalone processing. Within this framework, a momentum-accelerated gradient tracking method enables fully decentralized onboard estimation over a dynamic network and converges rapidly to the centralized benchmark solution. Overall, the proposed framework supports scalable and network-driven GNSS processing for large-scale LEO constellations, enabling high-precision onboard navigation through cooperative estimation in space.

ACKNOWLEDGEMENTS

The authors would like to thank Prof. Peter J. G. Teunissen for conceptual suggestions and valuable discussions on distributed GNSS processing, which helped shape the initial direction of this work.

APPENDIX A

SUBMATRIX DEFINITIONS OF THE DESIGN MATRIX

This appendix provides the block-wise definitions of the submatrices that together form the overall design matrix \mathbf{A} .

• LEO orbit-related design matrix:

$$\mathbf{A}_{\text{leo-orb}} = \text{blkdiag}_{l=1}^L (\mathbf{H}_l^{\text{leo-orb}}), \quad (\text{A.1})$$

where

$$\mathbf{H}_l^{\text{leo-orb}} = \begin{bmatrix} \mathbf{H}_{l,1}^{\text{leo-orb}} \\ \vdots \\ \mathbf{H}_{l,F}^{\text{leo-orb}} \end{bmatrix}, \mathbf{H}_{l,f}^{\text{leo-orb}} = \begin{bmatrix} \mathbf{U}_l & \mathbf{0} \\ \mathbf{U}_l & \mathbf{0} \\ \mathbf{0} & -\frac{1}{\lambda_f} \mathbf{U}_l \end{bmatrix}. \quad (\text{A.2})$$

Here, $\mathbf{U}_l \in \mathbb{R}^{G_l \times 3}$ is the LOS direction matrix for receiver l , with each row representing the LOS unit vector to a visible GNSS satellite.

• LEO clock and hardware-related design matrix:

$$\mathbf{A}_{\text{leo-clk}} = \text{blkdiag}_{l=1}^L (\mathbf{H}_l^{\text{leo-clk}}), \quad (\text{A.3})$$

with

$$\mathbf{H}_l^{\text{leo-clk}} = \begin{bmatrix} \mathbf{H}_{l,1}^{\text{leo-clk}} \mathbf{C}_1^{\text{freq}} \\ \vdots \\ \mathbf{H}_{l,F}^{\text{leo-clk}} \mathbf{C}_F^{\text{freq}} \end{bmatrix}, \mathbf{H}_{l,f}^{\text{leo-clk}} = \begin{bmatrix} 1 & 0 & \lambda_f & 0 \\ 1 & 0 & 0 & 1 \\ 0 & -\frac{1}{\lambda_f} & 0 & 0 \end{bmatrix} \otimes \mathbf{1}_{G_l}, \quad (\text{A.4})$$

where $\mathbf{C}_f^{\text{freq}}$ selects, from $\mathbf{x}_{\text{leo-clk}}^{(l)}$, the receiver clock and hardware-bias states associated with frequency f , and \otimes denotes the Kronecker product.

• GNSS clock and hardware-related design matrix:

$$\mathbf{A}_{\text{gnss-clk}} = -\text{col}_{l=1}^L (\mathbf{H}_l^{\text{gnss-clk}}), \quad (\text{A.5})$$

where

$$\mathbf{H}_l^{\text{gnss-clk}} = \text{col} \{ \mathbf{H}_{l,1}^{\text{gnss-clk}}, \dots, \mathbf{H}_{l,F}^{\text{gnss-clk}} \}, \quad (\text{A.6})$$

with

$$\mathbf{H}_{l,f}^{\text{gnss-clk}} = \text{col} \{ \mathbf{S}_{l,f}^{\phi}, \mathbf{S}_{l,f}^{\rho}, \mathbf{S}_{l,f}^d \}, \quad (\text{A.7})$$

$$\mathbf{S}_{l,f}^{\phi} = \text{col}_{g \in \mathcal{G}_l} (\mathbf{e}_g^{\top} \otimes \mathbf{s}_{l,f}^{\phi,g}), \quad (\text{A.8})$$

$$\mathbf{S}_{l,f}^{\rho} = \text{col}_{g \in \mathcal{G}_l} (\mathbf{e}_g^{\top} \otimes \mathbf{s}_{l,f}^{\rho,g}), \quad (\text{A.9})$$

$$\mathbf{s}_{l,f}^d = \text{col}_{g \in \mathcal{G}_l} (\mathbf{e}_g^\top \otimes \mathbf{s}_{l,f}^{d,g}), \quad (\text{A.10})$$

$$\mathbf{s}_{l,f}^{\phi,g} = [1, 0, \lambda_f \mathbf{e}_f^\top, \mathbf{0}_{1 \times F}], \quad (\text{A.11})$$

$$\mathbf{s}_{l,f}^{\rho,g} = [1, 0, \mathbf{0}_{1 \times F}, \mathbf{e}_f^\top], \quad (\text{A.12})$$

$$\mathbf{s}_{l,f}^{d,g} = \left[0, -\frac{1}{\lambda_f}, \mathbf{0}_{1 \times F}, \mathbf{0}_{1 \times F} \right]. \quad (\text{A.13})$$

Here, $\mathbf{e}_f \in \mathbb{R}^F$ denotes the f -th canonical basis vector, i.e., a vector with a 1 in position f and zeros elsewhere.

• **Ionosphere-related design matrix:**

$$\mathbf{A}_{\text{ion}} = \text{blkdiag}_{l=1}^L (\mathbf{H}_l^{\text{ion}}) \quad (\text{A.14})$$

where

$$\mathbf{H}_l^{\text{ion}} = \begin{bmatrix} \mathbf{H}_{l,1}^{\text{ion}} \\ \vdots \\ \mathbf{H}_{l,F}^{\text{ion}} \end{bmatrix}, \quad \mathbf{H}_{l,f}^{\text{ion}} = \begin{bmatrix} -\mu_f \\ +\mu_f \\ 0 \end{bmatrix} \otimes \mathbf{I}_{G_l}. \quad (\text{A.15})$$

• **Integer ambiguity-related design matrix:**

$$\mathbf{A}_{\text{amb}} = \text{blkdiag}_{l=1}^F (\mathbf{H}_l^{\text{amb}}), \quad (\text{A.16})$$

with

$$\mathbf{H}_l^{\text{amb}} = \text{blkdiag}_{f=1}^F (\mathbf{H}_{l,f}^{\text{amb}}), \quad \mathbf{H}_{l,f}^{\text{amb}} = \begin{bmatrix} \lambda_f \\ 0 \\ 0 \end{bmatrix} \otimes \mathbf{I}_{G_l}. \quad (\text{A.17})$$

APPENDIX B

MATRICES USED FOR RANK-DEFICIENCY ELIMINATION

This appendix presents the matrices that underpin the \mathcal{S} -system transformation. For convenience, we summarize several notations that will be used throughout this appendix: $\mathbf{c}_n = [1, 0, \dots, 0]^\top$, $\mathbf{1}_n = [1, 1, \dots, 1]^\top$, $\mathbf{D}_n = [-\mathbf{1}_n \quad \mathbf{I}_{n-1}]^\top$, $\mathbf{C}_n = [\mathbf{0}_{n-1} \quad \mathbf{I}_{n-1}]^\top$, $\mathbf{F}_n = [\mathbf{0}_{(n-2) \times 2} \quad \mathbf{I}_{n-2}]^\top$, $\mathbf{E}_n = \mathbf{C}_n \mathbf{D}_n^\top = \mathbf{I}_n - \mathbf{1}_n \mathbf{c}_n^\top$, $\boldsymbol{\mu} = [\mu_1, \dots, \mu_F]^\top$, $\boldsymbol{\mu}_{\text{IF}} = \frac{1}{\mu_2 - \mu_1} [\mu_2, -\mu_1, 0, \dots, 0]^\top$, $\boldsymbol{\mu}_{\text{GF}} = \frac{1}{\mu_2 - \mu_1} [-1, 1, 0, \dots, 0]^\top$, $\boldsymbol{\lambda} = [\lambda_1, \dots, \lambda_F]^\top$, and $\boldsymbol{\Lambda} = \text{diag}\{\lambda_1, \dots, \lambda_F\}$.

The matrices employed to eliminate the rank deficiencies are defined in (B.1) to (B.4). The ambiguity-related blocks are constructed based on the receiver–satellite visibility sets and the adopted pivot selection, and therefore do not admit a universal closed-form expression; their role is to eliminate the ambiguity-related rank deficiencies under the chosen \mathbf{S} -basis. For compactness, we omit the explicit listing of these graph-dependent blocks and instead summarize their role in Table I/Table II.

REFERENCES

- [1] X. Lin, S. Cioni, G. Charbit, N. Chuberre, S. Hellsten, and J.-F. Boutilhon, “On the path to 6G: Embracing the next wave of low Earth orbit satellite access,” *IEEE Communications Magazine*, vol. 59, no. 12, pp. 36–42, 2021.
- [2] L. You, K.-X. Li, J. Wang, X. Gao, X.-G. Xia, and B. Ottersten, “Massive MIMO transmission for LEO satellite communications,” *IEEE Journal on Selected Areas in Communications*, vol. 38, no. 8, pp. 1851–1865, 2020.
- [3] S. Liu, Z. Gao, Y. Wu, D. W. Kwan Ng, X. Gao, K.-K. Wong, S. Chatzinotas, and B. Ottersten, “LEO satellite constellations for 5G and beyond: How will they reshape vertical domains?” *IEEE Communications Magazine*, vol. 59, no. 7, pp. 30–36, 2021.
- [4] T. G. Reid, M. Gala, M. Favreau, A. Kriezis, M. O’Meara, A. Pant, P. Tarantino, and C. Youn, “Xona Pulsar compatibility with GNSS,” in *Proceedings of the 38th International Technical Meeting of the Satellite Division of The Institute of Navigation (ION GNSS+ 2025)*, 2025, pp. 929–943.
- [5] M. Hui, S. Zhai, D. Wang, T. Hui, W. Wang, P. Du, and F. Gong, “A review of LEO-satellite communication payloads for integrated communication, navigation, and remote sensing: Opportunities, challenges, future directions,” *IEEE Internet of Things Journal*, vol. 12, no. 12, pp. 18954–18992, 2025.
- [6] M. Lv, X. Peng, W. Xie, and N. Guan, “Task allocation for real-time earth observation service with LEO satellites,” in *2022 IEEE Real-Time Systems Symposium (RTSS)*, 2022, pp. 14–26.
- [7] K. Selvan, A. Siemuri, F. S. Prol, P. Välijuo, M. Z. H. Bhuiyan, and H. Kuusniemi, “Precise orbit determination of LEO satellites: a systematic review,” *GPS Solutions*, vol. 27, no. 4, p. 178, 2023.
- [8] A. Allahvirdi-Zadeh, K. Wang, and A. El-Mowafy, “Precise orbit determination of LEO satellites based on undifferenced GNSS observations,” *Journal of surveying engineering*, vol. 148, no. 1, p. 03121001, 2022.
- [9] G. Nie, F. Wu, K. Zhang, and B. Zhu, “Research on LEO satellites time synchronization with GPS receivers onboard,” in *2007 IEEE International Frequency Control Symposium Joint with the 21st European Frequency and Time Forum*, 2007, pp. 896–900.
- [10] O. Montenbruck, F. Kunzi, F. D. O. Salgueiro, F. Gini, and M. C. Limón, “GNSS-based synchronization and monitoring of LEO-PNT onboard time,” *Advances in Space Research*, 2025.
- [11] O. Montenbruck, E. Gill, and R. Kroes, “Rapid orbit determination of LEO satellites using IGS clock and ephemeris products,” *GPS Solutions*, vol. 9, no. 3, pp. 226–235, 2005.
- [12] P. Héroux and J. Kouba, *GPS precise point positioning with a difference*. Natural Resources Canada, Geomatics Canada, Geodetic Survey Division Ottawa …, 1995.
- [13] J. F. Zumberge, M. B. Heflin, D. C. Jefferson, M. M. Watkins, and F. H. Webb, “Precise point positioning for the efficient and robust analysis of GPS data from large networks,” *Journal of geophysical research: solid earth*, vol. 102, no. B3, pp. 5005–5017, 1997.
- [14] G. Wabben, M. Schmitz, and A. Bagge, “PPP-RTK: precise point positioning using state-space representation in RTK networks,” in *Proceedings of the 18th international technical meeting of the satellite division of the Institute of navigation (ION GNSS 2005)*, 2005, pp. 2584–2594.
- [15] B. Hofmann-Wellenhof, H. Lichtenegger, and E. Wasle, *GNSS—global navigation satellite systems: GPS, GLONASS, Galileo, and more*. Springer, 2008.
- [16] J. M. Palomo, P. D’angelo, P. Silva, A. Fernández, P. Giordano, P. Zoccarato, J. Tegedor, O. Oerpen, L. Hansen, C. Hill *et al.*, “Space GNSS receiver performance results with precise real-time on-board orbit determination (P2OD) in LEO missions,” in *Proceedings of the 32nd International Technical Meeting of the Satellite Division of The Institute of Navigation (ION GNSS+ 2019)*, 2019, pp. 1172–1186.
- [17] J. Pi, Y. Ran, H. Wang, Y. Zhao, R. Zhao, and J. Luo, “Dynamic planning of inter-plane inter-satellite links in LEO satellite networks,” in *ICC 2022 - IEEE International Conference on Communications*, 2022, pp. 3070–3075.
- [18] C. Wu, S. Han, Q. Chen, Y. Wang, W. Meng, and A. Benslimane, “Enhancing LEO mega-constellations with inter-satellite links: Vision and challenges,” *IEEE Wireless Communications*, vol. 32, no. 5, pp. 196–202, 2025.
- [19] A. H. Sayed, “Diffusion adaptation over networks,” in *Academic Press Library in Signal Processing*. Elsevier, 2014, vol. 3, pp. 323–453.
- [20] R. Olfati-Saber, J. A. Fax, and R. M. Murray, “Consensus and cooperation in networked multi-agent systems,” *Proceedings of the IEEE*, vol. 95, no. 1, pp. 215–233, 2007.
- [21] X. Zhao and A. H. Sayed, “Asynchronous adaptation and learning over networks—part i: Modeling and stability analysis,” *IEEE Transactions on Signal Processing*, vol. 63, no. 4, pp. 811–826, 2015.
- [22] B. McMahan, E. Moore, D. Ramage, S. Hampson, and B. A. y Arcas, “Communication-efficient learning of deep networks from decentralized data,” in *Artificial intelligence and statistics*. PMLR, 2017, pp. 1273–1282.
- [23] T. Yang, X. Yi, J. Wu, Y. Yuan, D. Wu, Z. Meng, Y. Hong, H. Wang, Z. Lin, and K. H. Johansson, “A survey of distributed optimization,” *Annual Reviews in Control*, vol. 47, pp. 278–305, 2019.
- [24] W. Baarda, “S-transformations and criterion matrices,” *Netherlands geodetic commission*, 1973.

$$\mathbf{V} = \begin{bmatrix} \mathbf{0} & \mathbf{0} & \mathbf{0} & \mathbf{0} & \mathbf{0} & \mathbf{0} \\ \mathbf{1}_L \otimes \mathbf{I}_{2F+2} & \mathbf{C}_L \otimes \begin{bmatrix} -1 \\ 0 \\ \Lambda^{-1} \mathbf{1}_F \end{bmatrix} & \mathbf{0} & \mathbf{C}_L \otimes \begin{bmatrix} 0 \\ 0 \\ -\mu \end{bmatrix} & \mathbf{0} & \mathbf{0} \\ \mathbf{1}_G \otimes \mathbf{I}_{2F+2} & \mathbf{0} & \mathbf{I}_G \otimes \begin{bmatrix} -1 \\ 0 \\ \Lambda^{-1} \mathbf{1}_F \end{bmatrix} & \mathbf{0} & \mathbf{I}_G \otimes \begin{bmatrix} 0 \\ 0 \\ \mu \end{bmatrix} & -\mathbf{C}_L \otimes \begin{bmatrix} 0 \\ 0 \\ \mathbf{I}_F \end{bmatrix} \\ \mathbf{0} & \mathbf{0} & \mathbf{0} & \begin{bmatrix} \mathbf{0} & \mathbf{0} & \cdots & \mathbf{0} \\ \mathbf{1}_{G_2} & \mathbf{0} & \cdots & \mathbf{0} \\ \mathbf{0} & \mathbf{1}_{G_3} & \cdots & \mathbf{0} \\ \vdots & & & \mathbf{0} \\ \mathbf{0} & \mathbf{0} & \cdots & \mathbf{1}_{G_L} \end{bmatrix} & \begin{bmatrix} \mathbf{I}_G(\mathcal{G}_1, :) \\ \mathbf{I}_G(\mathcal{G}_2, :) \\ \vdots \\ \mathbf{I}_G(\mathcal{G}_L, :) \end{bmatrix} & \mathbf{0} \\ \mathbf{0} & \mathbf{0} & \mathbf{0} & \mathbf{0} & \mathbf{0} & \begin{bmatrix} \mathbf{I}_F \otimes \mathbf{1}_{G_2} & \mathbf{0} & \cdots & \mathbf{0} \\ \mathbf{0} & \mathbf{I}_F \otimes \mathbf{1}_{G_3} & \cdots & \mathbf{0} \\ \vdots & & & \mathbf{0} \\ \mathbf{0} & \mathbf{0} & \cdots & \mathbf{I}_F \otimes \mathbf{1}_{G_L} \end{bmatrix} \\ \mathbf{0} & \mathbf{0} & \mathbf{0} & \mathbf{0} & \begin{bmatrix} \mathbf{I}_F \otimes \mathbf{I}_G(\mathcal{G}_1, :) \\ \mathbf{I}_F \otimes \mathbf{I}_G(\mathcal{G}_2, :) \\ \vdots \\ \mathbf{I}_F \otimes \mathbf{I}_G(\mathcal{G}_L, :) \end{bmatrix} & \mathbf{0} \end{bmatrix} \quad (\text{B.1})$$

$$(\mathbf{S}^\perp)^T = \begin{bmatrix} \mathbf{0} & \mathbf{c}_L^T \otimes \mathbf{I}_{2F+2} & \mathbf{0} & \mathbf{0} \\ \mathbf{0} & \mathbf{D}_L^T \otimes (\mathbf{0}_{1 \times (F+2)} \ \mu_{\text{IF}}^T) & \mathbf{0} & \mathbf{0} \\ \mathbf{0} & -(\mathbf{c}_L^T \otimes \mathbf{1}_G) \otimes (\mathbf{0}_{1 \times (F+2)} \ \mu_{\text{IF}}^T) & \mathbf{I}_G \otimes (\mathbf{0}_{1 \times (F+2)} \ \mu_{\text{IF}}^T) & \mathbf{0} \\ \mathbf{0} & -\mathbf{D}_L^T \otimes (\mathbf{0}_{1 \times (F+2)} \ \mu_{\text{GF}}^T) & \mathbf{0} & \mathbf{0} \\ \mathbf{0} & -(\mathbf{c}_L^T \otimes \mathbf{1}_G) \otimes (\mathbf{0}_{1 \times (F+2)} \ \mu_{\text{GF}}^T) & \mathbf{I}_G \otimes (\mathbf{0}_{1 \times (F+2)} \ \mu_{\text{GF}}^T) & \mathbf{0} \\ \mathbf{0} & \mathbf{0} & \mathbf{0} & \mathbf{K}_{\text{rec-amb}} \\ \mathbf{0} & \mathbf{0} & \mathbf{0} & \mathbf{K}_{\text{sat-amb}} \end{bmatrix} \quad (\text{B.2})$$

$$\mathbf{S} = \begin{bmatrix} \mathbf{I}_{6L} & \mathbf{0} & \mathbf{0} & \mathbf{0} \\ \mathbf{0} & \mathbf{C}_L \otimes \begin{pmatrix} 1 & 0 & 0 & 0 \\ 0 & 1 & 0 & 0 \\ 0 & 0 & \mathbf{I}_F & 0 \\ 0 & 0 & 0 & \mathbf{F}_F \end{pmatrix} & \mathbf{0} & \mathbf{0} \\ \mathbf{0} & \mathbf{0} & \mathbf{I}_G \otimes \begin{pmatrix} 1 & 0 & 0 & 0 \\ 0 & 1 & 0 & 0 \\ 0 & 0 & \mathbf{I}_F & 0 \\ 0 & 0 & 0 & \mathbf{F}_F \end{pmatrix} & \mathbf{0} & \mathbf{0} \\ \mathbf{0} & \mathbf{0} & \mathbf{0} & \mathbf{I}_{\sum_l G_l} \\ \mathbf{0} & \mathbf{0} & \mathbf{0} & \mathbf{0} \end{bmatrix} \quad (\text{B.3})$$

$$\begin{aligned} \mathcal{S} &= \mathbf{I} - \mathbf{V} \left[(\mathbf{S}^\perp)^T \mathbf{V} \right]^{-1} (\mathbf{S}^\perp)^T = \mathbf{I} - \mathbf{V} (\mathbf{S}^\perp)^T = \\ &= \begin{bmatrix} \mathbf{I}_L \otimes \mathbf{I}_6 & \mathbf{0} & \mathbf{0} & \mathbf{0} \\ \mathbf{0} & \mathbf{I}_L \otimes \mathbf{I}_{2F+2} - (\mathbf{1}_L \mathbf{c}_G^T) \otimes \mathbf{I}_{2F+2} - \mathbf{E}_L \otimes \begin{pmatrix} \mathbf{0} & \mathbf{0} & \mathbf{0} & -\mu_{\text{IF}}^T \\ \mathbf{0} & \mathbf{0} & \mathbf{0} & \mathbf{0} \\ \mathbf{0} & \mathbf{0} & \mathbf{0} & \Lambda^{-1} \mathbf{1}_F \mu_{\text{IF}}^T - \Lambda^{-1} \mu \mu_{\text{GF}}^T \\ \mathbf{0} & \mathbf{0} & \mathbf{0} & 1_F \mu_{\text{IF}}^T + \mu \mu_{\text{GF}}^T \end{pmatrix} \\ \mathbf{0} & -(\mathbf{1}_G \mathbf{c}_L^T) \otimes \mathbf{I}_{2F+2} + (\mathbf{1}_L \mathbf{c}_G^T) \otimes \begin{pmatrix} \mathbf{0} & \mathbf{0} & -\mu_{\text{IF}}^T \\ \mathbf{0} & \mathbf{0} & \mathbf{0} \\ \mathbf{0} & \mathbf{0} & \Lambda^{-1} \mathbf{1}_F \mu_{\text{IF}}^T - \Lambda^{-1} \mu \mu_{\text{GF}}^T \\ \mathbf{0} & \mathbf{0} & 1_F \mu_{\text{IF}}^T + \mu \mu_{\text{GF}}^T \end{pmatrix} \\ \mathbf{0} & \begin{bmatrix} \mathbf{1}_{G_1} & \mathbf{0} & \cdots & \mathbf{0} \\ \mathbf{0} & \mathbf{1}_{G_2} & \cdots & \mathbf{0} \\ \vdots & & & \mathbf{0} \\ \mathbf{0} & \mathbf{0} & \cdots & \mathbf{1}_{G_L} \end{bmatrix} \otimes (\mathbf{0}_{1 \times (F+2)} \ \mu_{\text{GF}}^T) \\ \mathbf{0} & \end{bmatrix} \quad (\text{B.4}) \end{aligned}$$

- [25] P. Teunissen, “Zero order design: generalized inverses, adjustment, the datum problem and S-transformations,” in *Optimization and design of geodetic networks*. Springer, 1985, pp. 11–55.
- [26] D. Odijk, B. Zhang, A. Khodabandeh, R. Odolinski, and P. J. Teunissen, “On the estimability of parameters in undifferenced, uncombined GNSS network and PPP-RTK user models by means of S-system theory,” *Journal of Geodesy*, vol. 90, no. 1, pp. 15–44, 2016.
- [27] A. Nedic, A. Olshevsky, and W. Shi, “Achieving geometric convergence for distributed optimization over time-varying graphs,” *SIAM Journal on Optimization*, vol. 27, no. 4, pp. 2597–2633, 2017.
- [28] X. X. Zheng, X. Liu, and T. Y. Al-Naffouri, “Decentralized GNSS at global scale via graph-aware diffusion adaptation,” 2025, arXiv preprint.
- [29] R. Nassif, S. Vlaski, M. Carpentiero, V. Matta, and A. H. Sayed, “Differential error feedback for communication-efficient decentralized learning,” *IEEE Transactions on Signal Processing*, vol. 73, pp. 1905–1921, 2025.
- [30] X. X. Zheng, W. Liu, X. Lou, S. Vlaski, and T. Al-Naffouri, “Quantitative error feedback for quantization noise reduction of filtering over graphs,” *arXiv preprint arXiv:2506.01404*, 2025.
- [31] S. Vlaski, S. Kar, A. H. Sayed, and J. M. Moura, “Networked signal and information processing: Learning by multiagent systems,” *IEEE Signal Process. Mag.*, vol. 40, no. 5, pp. 92–105, 2023.
- [32] M. Coutino and G. Leus, “A cascaded structure for generalized graph filters,” *IEEE Transactions on Signal Processing*, vol. 70, pp. 3499–3513, 2022.
- [33] P. J. G. Teunissen, “The least-square ambiguity decorrelation adjustment: A method for fast GPS integer ambiguity estimation,” *Journal of Geodesy*, vol. 70, no. 1, pp. 65–82, 1995.